Evaluation of Weather Radar with Pulse Compression: Performance of a Fuzzy Logic Tornado Detection Algorithm

TIMOTHY A. ALBERTS AND PHILLIP B. CHILSON

School of Meteorology, and Atmospheric Radar Research Center, Norman, Oklahoma

B. L. CHEONG

Atmospheric Radar Research Center, Norman, Oklahoma

R. D. PALMER

School of Meteorology, and Atmospheric Radar Research Center, Norman, Oklahoma

(Manuscript received 19 October 2009, in final form 3 September 2010)

ABSTRACT

Trends in current weather research involve active phased-array radar systems that have several advantages over conventional radars with klystron or magnetron transmitters. However, phased-array radars generally do not have the same peak transmit power capability as conventional systems so they must transmit longer pulses to maintain an equivalent average power on target. Increasing transmits pulse duration increases range gate size but the use of pulse compression offers a means of recovering the otherwise lost resolution. To evaluate pulse compression for use in future weather radar systems, modifications to a weather radar simulator have been made to incorporate phase-coding into its functionality. Data derived from Barker-coded pulses with matched and mismatched filters were compared with data obtained from uncoded pulses to evaluate the pulse compression performance. Additionally, pulse compression was simulated using data collected from an experimental radar to validate the simulated results. The data derived from both experimental and simulated methods were then applied to a fuzzy logic tornado detection algorithm to examine the effects of the pulse compression process. It was found that the fuzzy logic process was sufficiently robust to maintain high levels of detection accuracy with low false alarm rates even though biases were observed in the pulse-compressed data.

1. Introduction

There is an increasing interest in utilizing active phased-array radar systems with lower-power aperture products in meteorological applications (Zrnić et al. 2007; Weber et al. 2007). This has led to examining methods that can recover lost sensitivity due to peak transmit power limitations resulting from the use of solid-state power amplifiers. One such method is pulse compression, which involves coding the transmitted signal in such a way that, upon decoding, the range resolution and signal detectability are enhanced (Skolnik 1990; Nathanson 1991). The technique is not without its drawbacks, in that it creates range–time sidelobes that can corrupt the desired main lobe signal as well as increasing the minimum range of the radar. These two effects, however, can be mitigated by using different types of codes that can vary, for example, in length, type, bandwidth, and sidelobe suppression. Of particular importance, greater sidelobe suppression, as described by the integrated sidelobe level (ISL), leads to more accurate estimation of meteorologically relevant products such as reflectivity and radial velocity.

In the present study, a phase-coding capability has been incorporated into a weather radar simulator to examine a small set of pulse compression schemes. Specifically, Barker phase codes with matched and mismatched filters have been evaluated to demonstrate the accuracy of such a system as well as investigating its applicability in tornado detection. Whereas matched filters are specifically

Corresponding author address: Timothy A. Alberts, Atmospheric Technology Services Company, 3100 Monitor Ave., Ste. 140, Norman, OK 73072.
E-mail: tim.alberts@atscwx.com

DOI: 10.1175/2010JTECHA1409.1

designed to maximize the signal-to-noise ratio of the backscattered signal, mismatched filters aim to suppress the effects of range–time sidelobes. Additionally, data obtained from an experimental weather radar were artificially phase coded to simulate pulse compression in order to validate the weather radar simulator results as well as to examine any additional effects that may be encountered in an operational environment.

Traditional tornado detection algorithms use shear signatures to determine the presence of a tornado. The method employed here utilizes traditional signatures in conjunction with spectral information to improve detection performance within the context of a fuzzy logic system. The fuzzy logic system is a simplified version of the Neuro-Fuzzy Tornado Detection Algorithm (NFTDA) proposed in (Wang et al. 2008) in that the neural network has been removed to stabilize comparisons between pulse compression methods.

The remaining portion of the paper is organized into four additional sections with the next section covering background information concerning pulse compression, simulation procedures, fuzzy logic tornado detection, and the performance evaluation methodology. The third section briefly describes the data collection methods while the fourth examines the results of the data collection from both the radar simulator and field data that have been modified to mimic phase coded data. The last section draws the conclusions from the study.

2. Background

a. Pulse compression

Pulse compression involves transmitting a wideband signal coded in either frequency or phase and decoding the return signal through filtering, which results in increased average transmit power and enhanced range resolution compared to an identical system that does not include pulse compression (Skolnik 1990). Phase codes partition the transmitted pulse into segments of equal time duration, or subpulses, and then switch the phase of the signal at specified segments. In particular, binary phase codes switch the phase between two values, usually 0 and π, 0 and 1, or + and −. The amount of compression possible is equivalent to the time–bandwidth product (BT) of the code, which is the product of the signal bandwidth and signal total duration. Bandwidth of a phase-coded signal is calculated with

$$B = \frac{1}{\tau}, \tag{1}$$

where τ is taken to be the code subpulse length. The return signal power increase is proportional to the code length while the range resolution is inversely related to bandwidth as given by

$$\Delta r = \frac{c}{2B}. \tag{2}$$

This shows that decreasing subpulse duration results in a corresponding enhancement in range resolution regardless of the total pulse length. See Skolnik (1990) and Nathanson (1991) for more details.

One problem with pulse compression is that it creates range sidelobes, artifacts produced by the compression process whereby returns from other ranges contaminate the signal at the desired range. This corruption alters the in-phase and quadrature (I and Q) time series data so that estimates based upon these data could be in error. Fortunately, sidelobe suppression filters can be included in the pulse compression scheme that reduce the amount of corruption in the data, resulting in more accurate estimations. This addition comes at the cost of a slightly decreased signal-to-noise ratio (SNR), increased minimum range, and increased complexity. The ISL metric indicates the amount of sidelobe corruption by comparing the total power contained within the sidelobes to the main lobe:

$$\mathrm{ISL} = 10 \log \sum_{i=1} \frac{x_i^2}{x_0^2}. \tag{3}$$

In this equation, x_0 refers to the main lobe magnitude while x_i refers to the ith-range sidelobe, with improvement being indicated by a reduction in its value. This metric is of great importance in meteorological applications since the backscattered signal is spread over several range gates. An attractive property of the Barker codes is that they have uniformly distributed sidelobes about the main lobe when decoded with a matched filter and have a mainlobe peak that is higher than the sidelobes by a factor equal to the code length (Skolnik 1990; Nathanson 1991). For example, a 5-bit Barker code in conjunction with a matched filter will produce a main lobe 5 times higher than the sidelobes. Errors also can be produced by targets with radial velocities that can alter the phase of the backscattered signal, but they are negligible at this transmitting frequency and pulse duration since the phase change is much less than 45° (Nathanson 1991). While other pulse compression schemes involve changing the transmitted pulse frequency, we have chosen to concentrate on binary phase coding.

b. Simulation procedure

The Time Series Weather Radar Simulator (TSWRS; Cheong et al. 2008) was used to create in-phase and

quadrature (I and Q) time series data for a case involving a tornadic supercell as modeled by the Advanced Regional Prediction System (ARPS; Xue et al. 2003). The TSWRS is a three-dimensional radar simulator consisting of an ensemble of thousands of scatterers placed within the field of view (i.e., all the radar resolution volumes along a radial) of the virtual radar. The meteorological fields used as input to the simulator correspond to output data from the ARPS numerical simulation model developed at the Center for the Analysis and Prediction of Storms (CAPS) at the University of Oklahoma. The spatial and temporal resolutions of the ARPS output used in this study were 25 m and 1 s, respectively. To begin the simulation process, scatterer characteristics are initialized from a known ARPS dataset where a scatterer can be thought of as a point target, which has been given properties that correspond to the meteorological parameters of a radar resolution volume. At the next time step, the scatterer positions are updated according to the wind field and their corresponding properties are also updated at their new locations. The return signal amplitude and phase from each scatterer are then processed via Monte Carlo integration to calculate time series of the desired meteorological signals. The I and Q data were then processed to calculate the velocity difference (ΔV), spectrum width (σ_v), spectral flatness (σ_s), phase of radially integrated bispectrum (P; Wang et al. 2008; Yu et al. 2007), and eigenratio (χ; Yeary et al. 2007) for use in a fuzzy logic tornado detection algorithm (FLTDA).

The simulation begins with the input of ARPS data into the TSWRS and the initialization of the scatterer properties. The simulations used 30 000 scatterers for the standard-resolution case while those incorporating pulse compression increased the number of scatterers proportionally to the increase in range resolution so that the same average scatterer density of 20 per resolution volume would be created. This scatterer density was chosen to balance computational speed with enough targets to create a realistic simulation of radar return signals. Next, the pulse is propagated throughout the radar field of view on a gate-by-gate basis, switching the phase code over the appropriate range gates. The radar then receives the returns from the scatterers and composes the signal. Mathematically, this step, taken from Mudukutore and Chandrasekar (1998), can be described by

$$y(i,j) = \sum_{\forall m+n-1=j} x_i(m,n). \tag{4}$$

After the signal is composed, the data are decoded through the filtering process to produce estimates of the reflectivity, radial velocity, and the parameters needed for input into the tornado detection algorithm using the covariance method (Doviak and Zrnić 1993). A graphical depiction of this process is shown in Fig. 1. An average signal-to-noise ratio of 70 dB was set for cases using the TSWRS to provide for a verification of the concept before evaluating it under more realistic conditions.

While the matched filter gives an impulse response that is a time-reversed replica of the transmitted signal (Cook and Bernfeld 1993), the mismatched filter operates on the output of the matched filter for this application. The mismatched filter was designed using the method from Key et al. (1959) for the 5- and 13-bit codes. The mismatched filter coefficients calculated from this process were then inserted into the simulation after matched filtering to provide for improved sidelobe suppression. The ISLs achieved are −8.0 and −18.8 dB for the 5-bit Barker code and −11.5 and −25.0 dB for the 13-bit Barker code using matched and mismatched filtering, respectively. The additional sidelobe suppression offered by the mismatched filters means that targets outside the range of interest would not have as large of a corrupting effect on the calculated parameters, such as reflectivity, for that particular range bin.

c. *Experimental weather radar procedure*

To validate the weather radar simulator results as well as examine any additional effects that may be encountered in an operational environment, data obtained from an experimental weather radar have been artificially phase coded to simulate pulse compression. The radar used in this experiment, is the prototype Weather Surveillance Radar-1988 Doppler (WSR-88D) at Norman, Oklahoma (KOUN), which has been modified to include dual-polarization (Doviak et al. 2002). Pulse compression was not used in the field data collection but rather was simulated by artificially switching the phase of the raw time series data over the appropriate number of range gates in accordance with the code. For example, a 13-bit Barker code pulse would extend over 13 range gates with the phase of the data being altered to replicate the code as it propagated throughout the radar field of view. The individual range gates were then summed to produce a composite signal that was then processed as in the radar simulator.

d. *Fuzzy logic tornado detection*

The tornado detection algorithm employed here is a modification of the NFTDA system proposed by Wang et al. (2008), derived from Yeary et al. (2007). The algorithm uses fuzzy logic that incorporates the five parameters previously mentioned, (gate-to-gate velocity change ΔV; spectrum width σ_v; spectral flatness σ_s; eigenratio χ; and phase of radially integrated bispectrum, PRIB or P), simultaneously in order to make a decision

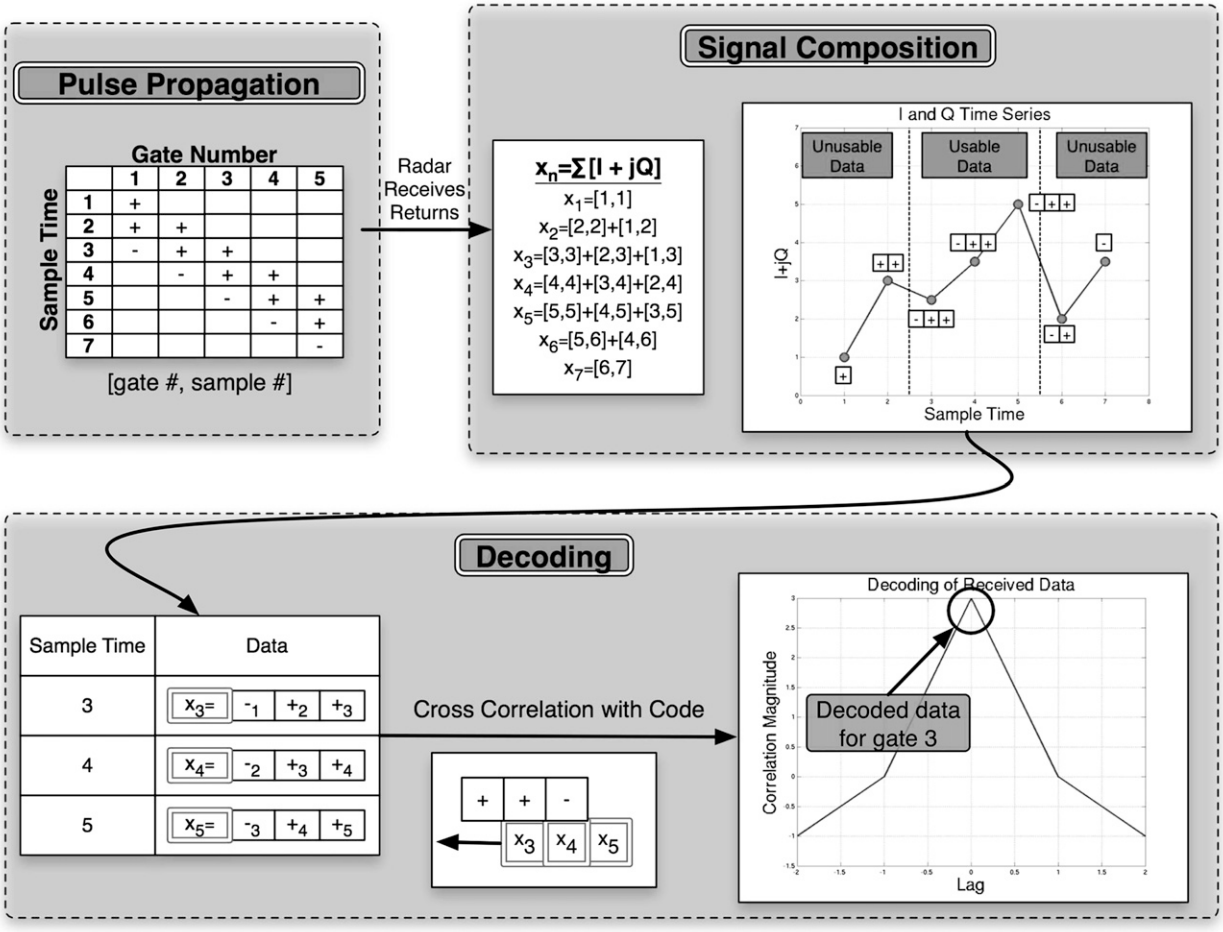

FIG. 1. Pulse compression decoding process with a matched filter. The phase code is propagated across the domain in time while the signals from each range gate are summed. The composite signal is then decoded using a matched filter to extract the desired data.

as to the existence of a tornado. To perform this function, the algorithm uses membership functions to denote the degree of membership in the ''yes'' or ''no'' set given a particular parameter value. The neural network has been removed from the process in order to stabilize comparisons between data obtained from nonpulse compression and pulse compression simulations. The neural network optimizes the membership functions to maximize the performance of the algorithm, which is counter to the intent here of simply comparing noncompressed and compressed results given a set of membership functions.

FLTDA utilizes the S- and Z-shaped membership functions in the fuzzification step, which can be described completely by a lower and an upper breaking point. Use of these one-sided membership functions implies that the input parameters can be described linguistically as being either ''high'' or ''low.'' The S-shaped membership function is given by

$$F_i^j(x)=\begin{cases}0 & x<x_1\\ 2\left(\dfrac{x-x_1}{x_2-x_1}\right)^2 & x_1\le x<\dfrac{x_1+x_2}{2}\\ 1-2\left(\dfrac{x-x_1}{x_2-x_1}\right)^2 & \dfrac{x_1+x_2}{2}\le x<x_2\\ 1 & x_2\le x\end{cases}, \quad (5)$$

where x_1 and x_2 represent the lower and upper breaking points, respectively; i is the input parameter; and j represents the tornadic or nontornadic case (Wang et al. 2008).

The rule inference step evaluates the strength of each rule, via the membership function results, in order to provide input into the defuzzification step. As in the NFTDA, the Mamdani system (Ross 2005) of rule inference was chosen, where the outputs of the fuzzification step are multiplied together to determine the rule strength. Defuzzification completes the process by simply using the maximum value

obtained from the rule inference process to make the final decision of whether or not a tornado is present.

e. Performance evaluation

The metrics used to describe the performance of the FLTDA are the same as those used in forecast verification (Murphy 1996). The process begins with the definition of a set of scenarios that describes the possible outcomes of the detection process. This is analogous to the construction of a 2×2 contingency table denoting hits, misses, false alarms, and nulls. A hit is defined as detecting a tornado within the area defined as containing a tornado. A miss is defined as not detecting a tornado when there was one present within the time step. A false alarm occurs when a tornado is detected outside of the area containing the tornado or if a detection is made when no tornado is present. The null state simply means that no detection was made when the tornado was not present. For each time step, or image, the location of the detections was compared to the area defined as containing the tornado when it was present. This area was defined as a circle having a radius of 200 m, which matched the estimated size of the vortex using ARPS data. The location of the tornado was determined by the location of the minimum pressure in the domain corresponding to the image. Formation of the tornado was determined to occur when a fully developed vortex formed in the density information at the lowest height of the ARPS simulation.

The performance of the algorithm was calculated over the entire simulation on a per image basis by calculating skill scores described below. The intent of the method was to analyze both the spatial and temporal levels of accuracy of the algorithm so that multiple hits and false detections for a single image were considered as one event. If a hit and a false detection were made for an image, then both events would be scored. This type of scoring led to sample sizes that could exceed the number of images for a simulation. The overall performance of the system could not be totally described by one metric, so four metrics were used consistent with that found in Mitchell et al. (1998). Shown below are the probability of detection (POD), false alarm ratio (FAR), critical success index (CSI), and the Heidke skill score (HSS) for each simulation (Wilks 2005):

$$\mathrm{POD} = \frac{a}{a+c}, \tag{6}$$

$$\mathrm{FAR} = \frac{b}{a+b}, \tag{7}$$

$$\mathrm{CSI} = \frac{a}{a+b+c}, \quad \text{and} \tag{8}$$

$$\mathrm{HSS} = \frac{2(ad-bc)}{(a+c)(c+d)+(a+b)(b+d)}. \tag{9}$$

In all of these equations, a is the number of hits, b is the number of false alarms, c is the number of misses, and d is the number of nulls.

The POD describes the likelihood of detecting an event given that the event occurs, with a score of 1 corresponding to perfect detection. The FAR is the ratio of false detections to total detections and is typically used in conjunction with POD. A score of 0 means that no false detections were made. CSI indicates the proportion of events correctly detected given that null cases are removed, where a score of 1 is perfect. Finally, the HSS measures the accuracy of the algorithm relative to that which would be detected by random chance. In other words, it calculates a score after removing hits that would have occurred solely by random chance.

The process of tornado detection and its performance hinges upon there being actual differences between tornadic and nontornadic signatures as well as the data collection method being able to accurately estimate those signatures. Brooks (2004) described a model for tornado-warning performance that is similar to the process defined here. The analogous point made was that greater separation between distributions generally leads to better performance. For the FLTDA, the distributions are those created for the five input parameters through sampling of the simulation. These distributions served as the foundation for defining the membership functions and adjusting them accordingly to improve detection performance. In terms of distributions, tornadic signatures typically have large gate-to-gate velocity differences, large spectrum widths, small spectral flatness, large eigenratios, and large PRIB.

The tornadic and nontornadic distributions of the parameters were created by setting a search area around the tornado and then dividing the signatures inside and outside of the search area between tornadic and nontornadic sets, respectively. This process was completed for all images, which were then summed to produce histograms of the signatures. The histograms were then used for comparison against the membership functions to examine the applicability of those breaking points to that simulation. If significant deviations between the membership functions and the histograms were found and believed to be a significant source of error, then the breaking points for those membership functions were adjusted. This process was repeated until the histograms and membership functions appeared to match in a qualitative sense.

3. Data collection

a. Weather radar simulator data

The test case for all simulations consisted of 99 images representing a small time segment of a tornadic supercell

TABLE 1. Error analysis for the 5-bit Barker code.

Parameter	Matched filter mean	Matched filter std dev	Mismatched filter mean	Mismatched filter std dev
ΔV (m s^{-1})	−0.07	1.46	−0.03	0.91
σ_s (dB)	−1.25	1.99	−1.18	1.73
χ	2×10^{-4}	22×10^{-4}	1×10^{-4}	12×10^{-4}
P (°)	0.22	3.02	0.16	2.68
σ_v (m s^{-1})	0.17	0.83	0.11	0.53
V_r (m s^{-1})	−0.02	1.14	-16×10^{-4}	0.72
Z (dB)	1.18	2.07	0.35	1.22

thunderstorm as modeled by the ARPS. Data were gathered using the TSWRS operating at 3.2 GHz. The pulse width was fixed at 1.57 μs with a pulse repetition interval of 1 ms, giving an unambiguous range and velocity of 150 km and 23.5 m s^{-1} respectively.

b. KOUN data

A tornado was tracked by KOUN on 10 May 2003 that provided I and Q data for volume scans at 0337, 0343, and 0349 UTC. The range resolution was 250 m with an unambiguous velocity of 35 m s^{-1} with data being gathered every 1° with a 1° beam resolution. During these times, the tornado was located approximately 40 km away from the radar and reached a maximum intensity of EF4 on the enhanced Fujita scale. Phase coding was accomplished by switching the phase of I and Q data over the appropriate number of range gates, which were then added together to simulate a long, coded pulse. Processing of the data was completed using the same method as that used for the TSWRS scenarios.

4. Experimental results

a. Weather radar simulator results

The TSWRS integrated a high-resolution dataset that contained a tornado within the simulated supercell thunderstorm. The radar range resolution was set to 235 m and served as the standard resolution definition. This resolution was chosen in order to maintain consistency with other informal studies that utilized the weather radar simulator. Due to computational limitations in terms of time, memory, and the extracted ARPS dataset, it was not possible to simulate Barker codes that would recover range resolution to 235 m. This forced the analysis to take the approach of comparing results between uncoded and coded data with smaller range gate spacing (i.e., finer resolution).

The pulse compression process correlates the return signals in range since the pulse extends over a number of range gates. The amount of interference impressed upon the desired signal from all the other range gates is expressed through the ISL. Therefore, a reduction in ISL should produce more accurate estimates of meteorological parameters such as reflectivity. Indeed, this is the case as is shown in Table 1, which presents the mean and standard deviation of Z, v_r, and all five of the fuzzy logic parameters. However, it was found that many of the parameters displayed varying degrees of bias. One notable case was that for spectral flatness, which was observed to have a strong, negative bias. The root cause is that the pulse compression process acts as a weighted averaging process that serves to reduce the variance of the I and Q data. This implies that the results differ at the spectral level, as shown in Fig. 2 where the mismatched filter better approximates the uncoded spectrum. This effect on the input parameters is summarized in Table 2 where the biases are separated into tornadic and nontornadic cases.

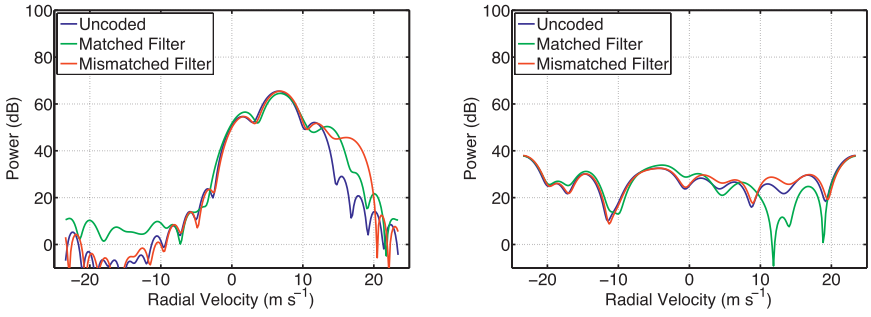

FIG. 2. Comparison of two tornadic spectra derived from uncoded and coded pulses.

TABLE 2. Average percent change in normalized histogram statistics for coded signatures using a 200-m search radius.

Parameter	Tornadic mean	Tornadic std dev	Nontornadic mean	Nontornadic std dev
ΔV (m s^{-1})	−11.0	−8.5	2.4	0.7
σ_s (dB)	−19.8	−22.2	−6.0	0.2
χ	57.7	27.9	9.0	16.1
P (°)	2.7	2.0	1.4	0.4
σ_v (m s^{-1})	20.5	5.0	7.7	8.9

The statistics were averaged for both matched and mismatched filters with a majority of the bias deriving from the matched filter cases. Of note, it was found that the errors for tornadic cases showed a greater error than nontornadic cases. The PRIB was the only parameter that did not demonstrate any bias in excess of 10%, while the eigenratio exhibited a strong positive bias for both tornadic and nontornadic signatures.

A contour plot of error in estimating Z using both matched and mismatched filters is shown in Fig. 3. The contour plots are normalized using the logarithm of the data to bring out the fine details. The x axis is the uncoded reflectivity gradient calculated along a radial, which has been smoothed by a rectangular window, in other words, a 13-point moving average. The first point to be made is that while decreasing ISL only reduces the mean error slightly, it does significantly reduce the variation of the error considerably over a wide band of gradients. The second point is that the error is asymmetric about both horizontal and vertical axes. While a complete explanation for this behavior is not proposed here, the asymmetry in error (i.e., about the 0-dBZ axis) may be due to the sidelobe structure of the code. The 13-bit as well as the 5-bit Barker codes are the only two code of this type that have all positive sidelobes, implying that the code would be biased toward overestimating the reflectivity since any interference would be additive. The asymmetry in the vertical direction (i.e., about the 0 dBZ m^{-1} axis) could simply be due to the simulation not containing enough samples that had a strong positive reflectivity gradient to show up in the data. To put the scale into perspective, a value of 0.1 corresponds to roughly 5 out of the 600 000 total points calculated.

Separating the signatures between tornadic and nontornadic cases resulted in Fig. 4, where some clear distinctions can be made between parameters. Most of the nontornadic signatures have a ΔV of less than 10 m s^{-1} while the tornadic signatures range fairly uniformly in value from 20 to over 40 m s^{-1}. For spectral flatness, the nontornadic signatures tend to increase in frequency starting at around 10 dB, peaking at about 20 dB, and then trailing off by about 25 dB. A less clear example is that for PRIB, where the tornadic and nontornadic signatures

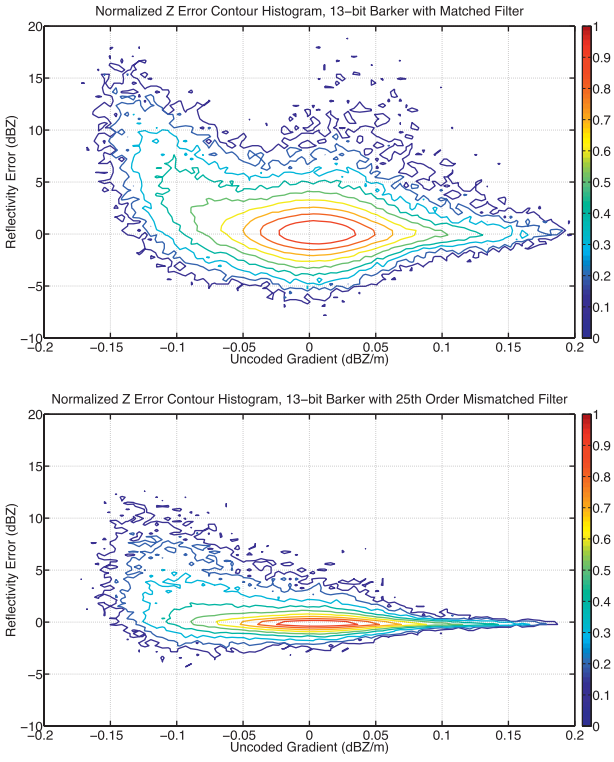

FIG. 3. Error contours for (top) matched and (bottom) mismatched filters with a 13-bit Barker code.

exhibit a Gaussian shape with the only difference being that the tornadic signatures have a slightly higher frequency at higher PRIBs.

Detection statistics of the FLTDA process that utilize ΔV, spectrum width, and spectral flatness as the input parameters are shown in Table 3. High POD, CSI, and HSS are coupled with a low FAR as is desired. The membership functions were manually optimized to maximize the performance of the algorithm for the matched filter case. Although the matched filter data have been shown to be less accurate than those derived from the mismatched filter, they can still produce high levels of performance. The reason being that the fuzzy logic approach leverages differences between distributions separately from the accuracy of the data resulting in essentially a decoupled problem. Greater separation between the tornadic and nontornadic signatures generally improves performance. It was also found that not all information inserted into the process improved performance. Some of the distributions, such as PRIB, have significant overlap between the two types of signatures that can result in erroneous classification. Examining Table 3 again shows that the mismatched filter performs worse than the matched filter. The cause is that the mismatched filter has several ‘‘misses’’ in its simulation that can be

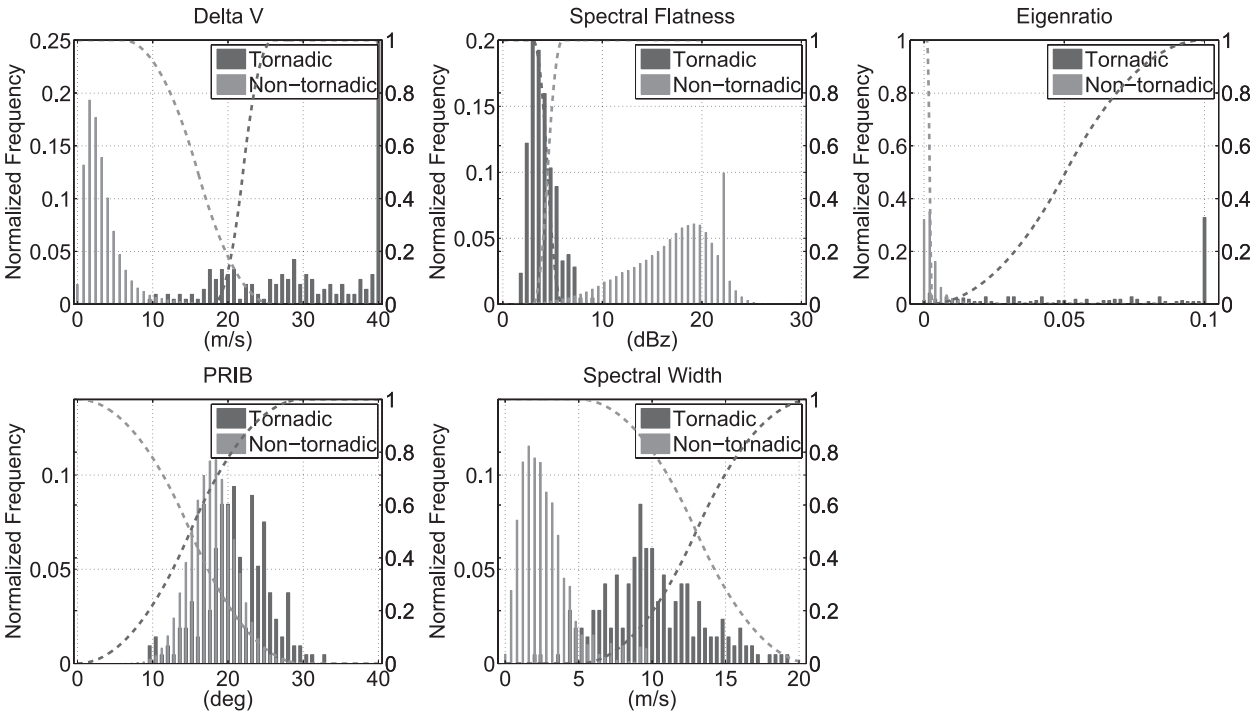

FIG. 4. Normalized histogram of signatures using a 5-bit Barker code with matched filtering in the TSWRS. The search radius was set to 50 m and the membership functions for the yes and 'no sets are represented by the dashed lines. Performance improved greatly as the distinction between histograms became clearer and the breaking points were adjusted accordingly.

attributed to small ΔV's that serve to nullify the other "hit" results.

b. KOUN results

Processing data obtained from KOUN in a similar manner as for the simulator, the algorithm detected the tornado at the appropriate locations in the three volume scans as demonstrated in Figs. 5 and 6. However, the algorithm did not successfully detect the tornado at 0337 UTC using 5- and 13-bit Barker codes with their respective mismatched filters. Suppression of the eigenratio at locations coincident with other tornadic indicators appears to be the cause of these misses. The algorithm did detect the tornado for all other cases regardless of processing method. While locating the tornado was successful, the number of detections resulting from pulse compression increased for most cases compared to that obtained without pulse compression. Reducing the ISL appears to alleviate this issue although this may be an artifact of the small number of samples used. The other item of note is that the PRIB is suppressed from the values obtained without pulse compression. It is unknown at this time as to the root cause of this observation, but the overall structure of the PRIB field is retained for all cases, which still makes it useful as a discriminator in the FLTDA process.

5. Conclusions

The transition from high peak power transmitters to low peak power transmit/receive modules in active multifunction phased-array radars provides significant challenges and opportunities for enhancing weather radar. One of these challenges is the recovery of lost range resolution due to the extension of the transmitted pulse in order to maintain detectability. This problem can be overcome through pulse compression techniques as has been demonstrated. TSWRS has been successfully modified to incorporate Barker phase coding into its operation. The integration of these two capabilities creates a flexible platform from which pulse compression studies can be conducted. Pulse compression, however, is not without drawbacks; most notable is the creation of range–time sidelobes that act to corrupt data at the desired range. This interference can be reduced through the use of sidelobe suppression filters as realized through the

TABLE 3. Detection statistics for FLTDA.

	Uncoded	Matched	Mismatched
POD	0.99	0.96	0.83
FAR	0.14	0.14	0.17
CSI	0.85	0.83	0.71
HSS	0.69	0.65	0.43

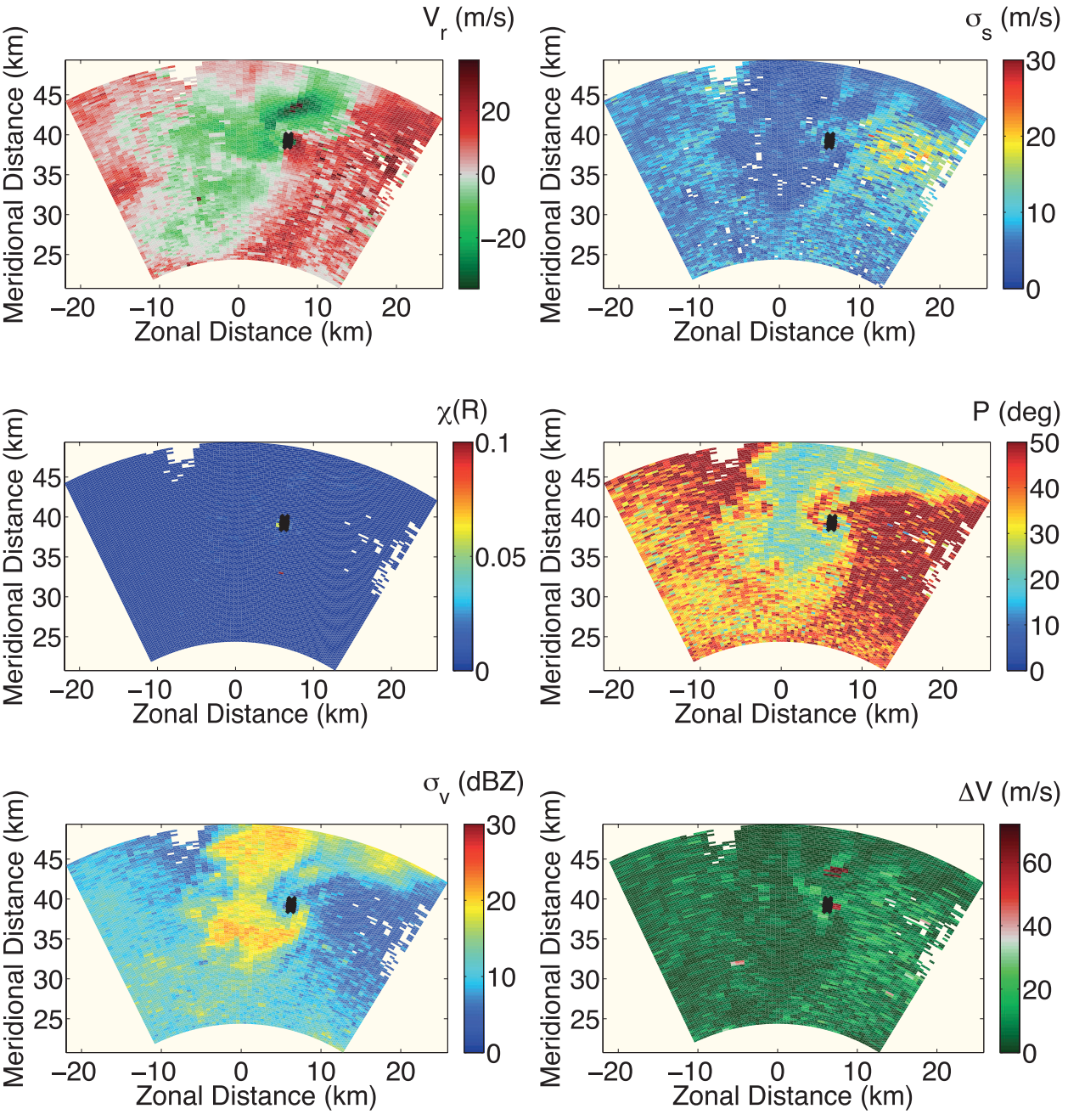

FIG. 5. Snapshot of the radial velocity and the five fuzzy logic input parameters used in the detection process derived from KOUN data taken at 0343 UTC. The black Xs indicate positive tornado detections by the algorithm using uncoded pulses. Shown are the (top left) radial velocity, (top right) spectral flatness, (middle left) eigenratio, (middle right) phase of the radially integrated bispectrum, (bottom left) spectrum width, and (bottom right) the gate-to-gate velocity change.

implementation of mismatched filters in this study. In weather applications the metric of interest is the ISL since weather echoes are widely distributed, and it has been shown that accuracy is improved as ISL is decreased. However, biases in the estimation of spectral parameters used in the FLTDA were observed, especially in spectral flatness. It seems plausible that most of these biases can be attributed to the range correlation effect and could be investigated further. Overall, there does not appear to be any strong negative effects from incorporating pulse compression into the simulated or actual radar system.

The use of a fuzzy logic system successfully integrated several parameters into a unified framework as applied to the tornado detection problem. The FLTDA performed

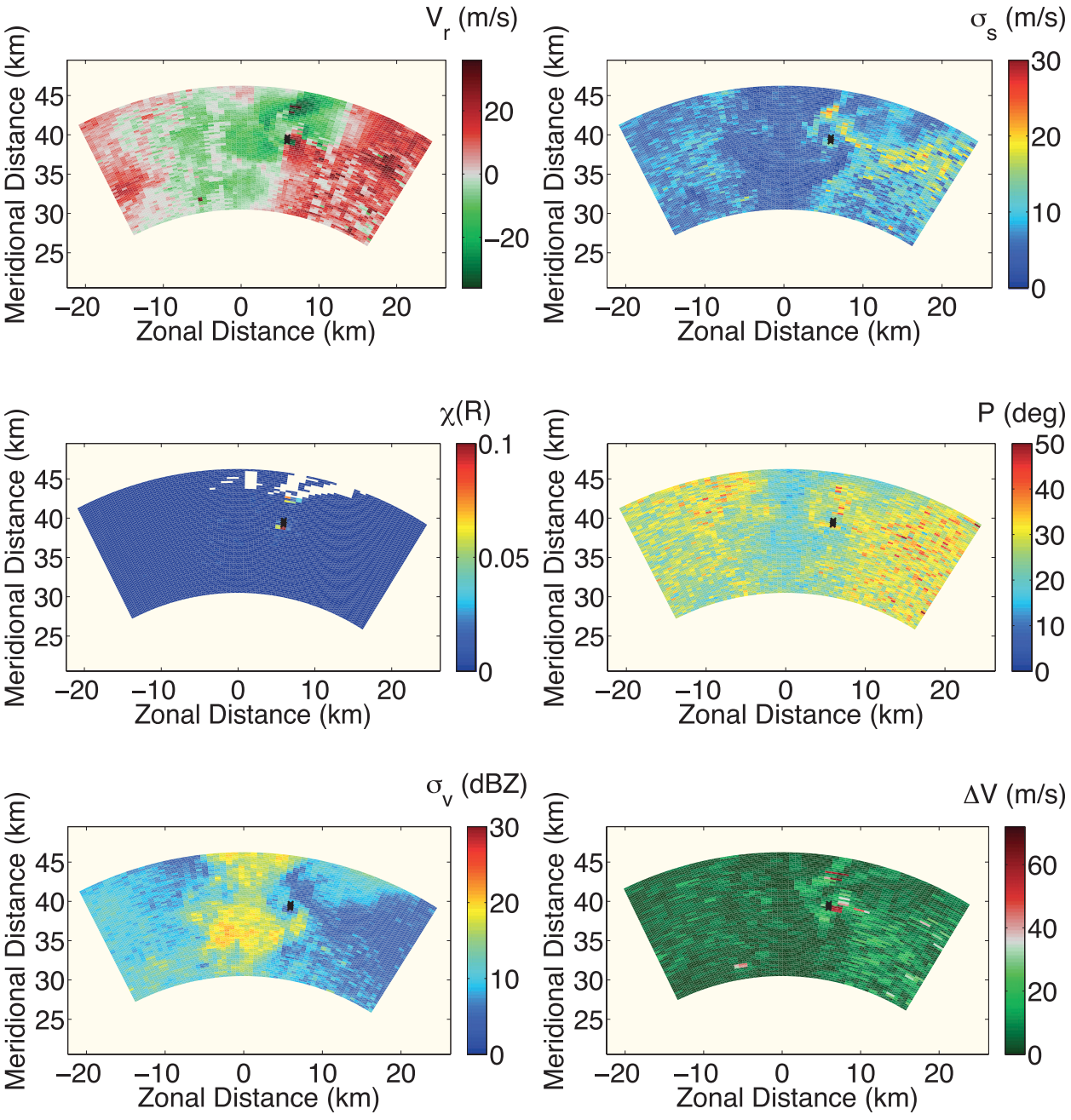

FIG. 6. As in Fig. 5, except this case uses a 13-bit Barker code with a mismatched filter.

very well in terms of POD, FAR, CSI, and HSS even with the observed biases in parameters due to the pulse compression process. It is believed that these biases will be eliminated with additional sidelobe suppression so that data obtained with coded pulses will be indistinguishable from data obtained with uncoded pulses. The fuzzy logic process was shown to adapt to a range of conditions through the altering of the breaking points of the membership functions, which allowed it to maintain a high level of performance. While a limited number of cases were used, there does not appear to be any problem with adjusting the fuzzy logic system to be successful over a wider range of conditions than the ones presented here. It was also shown that accurate estimation of a parameter does not imply improved detection performance but that detection performance relies on the presence of a consistent difference between signature types as well as the detection process being able to exploit those differences in the

most effective manner. Improvement may be possible by developing membership functions that can describe more complex shapes than the one-sided ones used here.

Acknowledgments. The authors thank the reviewers for their constructive critiques and time spent, which greatly improved the readability and content of this paper. We would also like to thank Tian-You Yu, Mark Yeary, Khoi Duc Le, and Yadong Wang for allowing us use of their data and for providing valuable advice in the creation of this paper. We would also like to acknowledge Tian-You Yu and Yadong Wang for sharing their methodology and experimental data. Funding for this project was provided under NOAA Cooperative Agreement NA17RJ1227.

REFERENCES

Brooks, H. E., 2004: Tornado-warning performance in the past and future: A perspective from signal detection theory. *Bull. Amer. Meteor. Soc.,* **85,** 837–843.

Cheong, B. L., R. D. Palmer, and M. Xue, 2008: A time-series weather radar simulator based on high-resolution atmospheric models. *J. Atmos. Oceanic Technol.,* **25,** 230–243.

Cook, C. E., and M. Bernfeld, 1993: *Radar Signals: An Introduction to Theory and Application.* Artech House, 531 pp.

Doviak, R. J., and D. S. Zrnić, 1993: *Doppler Radar and Weather Observations*. 2nd ed. Academic Press, 562 pp.

——, J. K. Carter, V. M. Melnikov, and D. S. Zrnić, 2002: Modifications to the research WSR-88D to obtain polarimetric data. NOAA/NSSL Tech. Rep., 49 pp.

Key, E. L., E. N. Fowle, and R. Haggarty, 1959: A method of side-lobe suppression in phase-coded pulse compression systems. Massachusetts Institute of Technology Tech. Rep. 209, 8 pp.

Mitchell, E. D., S. V. Vasiloff, G. J. Stumpf, A. Witt, M. D. Eilts, J. T. Johnson, and K. W. Thomas, 1998: The National Severe Storms Laboratory Tornado Detection Algorithm. *Wea. Forecasting,* **13,** 352–366.

Mudukutore, A. S., and V. Chandrasekar, 1998: Pulse compression for weather radars. *IEEE Trans. Geosci. Remote Sens.,* **36,** 125–142.

Murphy, A. H., 1996: The Finley affair: A signal event in the history of forecast verification. *Wea. Forecasting,* **11,** 3–20.

Nathanson, F. E., 1991: *Radar Design Principles*. 2nd ed. Prentice-Hall, 720 pp.

Ross, T. J., 2005: *Fuzzy Logic with Engineering Applications*. 2nd ed. John Wiley and Sons, 628 pp.

Skolnik, M. I., Ed., 1990: *Radar Handbook*. 2nd ed. McGraw Hill, 1200 pp.

Wang, Y., T.-Y. Yu, M. Yeary, A. Shapiro, S. Nemati, M. Foster, D. L. Andra Jr., and M. Jain, 2008: Tornado detection using a neuro-fuzzy system to integrate shear and spectral signatures. *J. Atmos. Oceanic Technol.,* **25,** 1136–1148.

Weber, M. E., J. Y. N. Cho, J. S. Herd, J. F. Flavin, W. E. Benner, and G. S. Torok, 2007: The next-generation multimission U.S. surveillance radar network. *Bull. Amer. Meteor. Soc.,* **88,** 1739–1751.

Wilks, D., 2005: *Statistical Methods in the Atmospheric Sciences*. 2nd ed. Academic Press, 627 pp.

Xue, M., D.-H. Wang, J.-D. Gao, K. Brewster, and K. K. Droegemeier, 2003: The Advanced Regional Prediction System (ARPS), storm-scale numerical weather prediction and data assimilation. *Meteor. Atmos. Phys.,* **82,** 139–170.

Yeary, M., S. Nemati, T.-Y. Yu, and Y. Wang, 2007: Tornadic time-series detection using Eigen analysis and a machine intelligence-based approach. *IEEE Geosci. Remote Sens. Lett.,* **4,** 335–339.

Yu, T.-Y., Y. Wang, A. Shapiro, M. B. Yeary, D. S. Zrnić, and R. J. Doviak, 2007: Characterization of tornado spectral signatures using higher-order spectra. *J. Atmos. Oceanic Technol.,* **24,** 1997–2013.

Zrnić, D. S., and Coauthors, 2007: Agile-beam phased array radar for weather observations. *Bull. Amer. Meteor. Soc.,* **88,** 1753–1766.